STUDY OF SILVER ADSORPTION ON CELLULOSE-BASED BIOSORBENTS

PAUNKA VASSILEVA,[*] IVAN UZUNOV,[*] DIMITRINKA VOYKOVA,[*] ANTONINA KOVACHEVA,[*] IVALINA AVRAMOVA,[*] GEORGI TYULIEV,[**] ROSITSA KUKEVA[*] and DIMITAR MEHANDJIEV[*]

[*]*Institute of General and Inorganic Chemistry, Bulgarian Academy of Sciences, Acad. G. Bonchev Str., bl. 11, 1113 Sofia, Bulgaria*
[**]*Institute of Catalysis, Bulgarian Academy of Sciences, Acad. G. Bonchev Str., bl. 11, 1113 Sofia, Bulgaria*
✉ *Corresponding author: P. Vassileva, pnovachka@svr.igic.bas.bg*

Received June 11, 2024

The survey aimed to investigate the adsorption properties of cellulose-based materials derived from cereal by-products towards Ag+ ions in water solutions, and to shed light on the mechanism of adsorption. Cellulose was isolated from rice and einkorn husks using alkali and bleaching treatments. Untreated einkorn husks and commercial cellulose served as reference samples. Characterization techniques included XRD, FTIR, SEM, and low-temperature nitrogen adsorption, with surface elemental composition analyzed by XPS. The study examined how contact time, initial silver ion concentration, pH, and temperature affected adsorption. The adsorption process was modeled using pseudo-second-order and Langmuir models, and thermodynamic parameters were evaluated. All materials showed potential as effective Ag+ ion adsorbents, indicating their suitability for creating silver-modified catalytic materials.

Keywords: adsorption, silver ions, cellulose, isotherm, thermodynamic

INTRODUCTION

Silver (Ag) is one of the naturally occurring noble metals and exhibits stability in acidic environments. It is widely used in various fields of engineering, especially in electronics.[1,2] Silver ions can enter water sources through industrial processes, medical and consumer products, as well as natural geological sources. The presence of silver ions in water, while less common than other heavy metals, still requires attention due to its potential adverse effects on both the environment and human health. The unbound ionic form of silver is recognized as among the most harmful metallic substances for aquatic life, including fish, phytoplankton, various invertebrates, and bacteria. Silver can hinder the activity of crucial enzymes involved in cellular metabolism by attaching to their sulfhydryl groups.[3,4] In its form of silver nitrate, $AgNO_3$, it is lethal to fish at very low concentrations, of 5–70 μg/L.[5,6]

On the other hand, when present in micro amounts, silver exhibits an oligo dynamic effect. This knowledge dates back to ancient times, when it found applications in both medicine and daily life for combating microbial pathogens. Consequently, silver ions are recognized for their antibacterial properties.[7,8]

The capture of silver ions from a water medium using low-cost natural biosorbents presents a promising and sustainable approach to water purification, while also enabling metal recycling. Moreover, doping micro-amounts of silver onto suitable supports leads to the development of materials with antiseptic properties.

Cellulose, a biodegradable and renewable polymer found abundantly in plants, offers various advantages as an adsorbent material for the removal of metal ions.[9-11] Its common presence in agricultural renewable residues makes it readily available and cost-effective compared to synthetic adsorbents. This abundance ensures a sustainable supply of cellulose-based adsorbents for water purification applications.[10-12] Additionally, cellulose-based adsorbents are biocompatible and environmentally friendly, posing minimal risks to human health and ecosystems. Unlike synthetic adsorbents, they are

non-toxic and biodegradable, ensuring minimal environmental impact during disposal. Last but not least, cellulose, which consists of β-glucosidic residues linked by oxygen bridges, possesses a large number of hydroxyl groups, which determine its affinity to metal ions. Overall, the use of cellulose-based adsorbents for the caption of silver ions from water media represents a promising strategy for sustainable water purification.

Renewable agricultural residues, derived from the milling industry, including materials like rice husks and einkorn husks are classified as lignocellulose materials, known for their widespread availability. These materials possess granular structure, diverse phase composition, chemical resilience, water resistance, and notable mechanical durability, making them ideal candidates for creating cost-effective natural biosorbents.[13-16] With their substantial cellulose content, they serve as a rich source of cellulose. Despite their potential, only a few researchers have explored the potential of natural rice husks as sorbents for removing silver ions.[1,17-19]

On the other hand, it is technologically and practically feasible that cellulose-based materials doped with Ag ions could serve as a base for creating materials, intended for removing septic pollution from biological solutions.[20,21]

In our previous research, we observed an increase in the amount of adsorbed silver on the investigated waste lignocellulose materials from bioethanol production correlating with their cellulose content.[22,23]

Considering circular economy principles, interest in converting renewable waste cellulosic materials into effective adsorbents is continuously growing. The structural features, mechanical and chemical resistance, and high mineral content of rice husks and einkorn husks make them attractive raw materials for obtaining adsorbents. Their use in the adsorption of various pollutants enhances the ecological impact of their processing. Currently, there is a lack of data in the literature on the use of cellulose derived from rice husks and einkorn husks for the adsorption of metals from aqueous media.

Therefore, the present study aims to assess and compare the effectiveness of various cellulose-based biosorbents derived from rice husks and einkorn husks in capturing silver ions from aqueous medium. Untreated raw einkorn husks and commercial microcrystalline cellulose were used as reference samples.

EXPERIMENTAL

Materials and methods

Materials

Rice husks from the 2022 harvest in the Pazardzhik region, Bulgaria (referred to as RH), and einkorn wheat husks sourced from the Haskovo region, Bulgaria (referred to as EH), were utilized. These husks were initially cleaned with deionized water and dried at 120 °C, before being milled using a rotary mill. The resulting fraction with particles smaller than 0.63 mm in size was selected for further use. Commercial microcrystalline cellulose powder (referred to as C) was procured from Sigma-Aldrich Co. Ltd.

Preparation of cellulose from rice husks and einkorn wheat husks

The cellulose extraction process from husks involved delignification and bleaching using NaOH and $NaOCl_2$, respectively. Initially, milled rice husks and einkorn husks were immersed in a solution containing NaOH and $NaHSO_3$ to eliminate hemicellulose and lignin. The mixture was stirred at 90 °C for 3 hours, followed by rinsing with deionized water until a neutral pH and drying in a vacuum oven at 60 °C for 24 hours. Subsequently, the resulting products underwent treatment in a solution containing $NaClO_2$ and acetic acid, stirred at 70 °C for 3 hours, to remove any residual lignin and hemicellulose. This bleaching step effectively disintegrates phenolic compounds and chromophore groups within the lignin molecules, thereby brightening the cellulose samples. Finally, the cellulose materials were dried once more in a vacuum oven at 60 °C for 24 hours and then ground into a powder with a particle size of less than 0.63 mm using a rotary mill. The obtained products were denoted as RHC – rice husk cellulose – and EHC – einkorn wheat husk cellulose.

Sample characterization

The phase composition of the materials was analyzed using powder X-ray diffraction. Diffractograms were obtained in the range of 5–80 degrees 2θ using a Bruker D8-Advance Diffractometer equipped with CuKα radiation and a LynxEye detector from Karlsruhe, Germany. Phase identification was facilitated using the EVA software package, which utilizes the ICDD-PDF-2(2021) database.

To examine the morphology of the samples, scanning electron microscopy (SEM) was employed using the JEOL JSM 6390 microscope in secondary electron image mode (SEI), applying the appropriate magnification.

Fourier-transform infrared spectra (FTIR) of the materials under investigation were obtained by mixing them with KBr. This mixture was then analyzed using a Thermo Nicolet Avatar 360 FTIR spectrometer manufactured by Thermo Fisher Scientific in Waltham, MA, USA. The instrument operated at a resolution of 2 cm^{-1}, allowing for detailed spectral analysis.

For the determination of texture parameters, low-temperature nitrogen adsorption at -196 °C was conducted using a Quantachrome Nova 1200e instrument from Anton Paar Quanta Tech Inc. The specific surface area was determined using the BET equation, while the total pore volumes and mean pore diameters were calculated at a relative pressure of approximately 0.99, following the Gurvitch rule. Pore-size distributions were determined using the BJH method.

The presence of adsorbed silver on the samples was investigated by X-ray photoelectron spectroscopy. The investigations were carried out using an ESCALAB MKII spectrometer with Al Kα (unmonochromatized) source at 1486.6 eV, with a total instrumental resolution of ~1 eV, under a base pressure of 10-8 mbarr. The Ag 3d photoelectron lines were recorded and calibrated for the C1s line at 285.0 eV. The XPSPEAK 4.0 fitting program was used for deconvolution of the photoelectron peaks. All the data were recorded at a 45° take-off angle.

Adsorption studies

Adsorption experiments were carried out using 50 mL conical flasks containing a predetermined quantity of adsorbent mixed with 10 mL of a silver ion solution. These mixtures were then agitated on a rotary shaker for varying durations. Subsequently, the solid particles were separated from the solution via filtration through a Millipore filter. The concentrations of silver ions were determined by inductively coupled plasma optical emission spectrometry (ICP-OES) on a Prodigy 7 ICP-OES spectrometer (Teledyne Leeman Labs, USA). A stock standard solution containing Ag+ ions at a concentration of 1000 mg L^{-1} was prepared using Titrisol (Merck, Germany) and subsequently diluted to achieve the desired pre-set initial concentrations. All reagents employed in the experiments were of analytical grade. Batch experiments were performed to explore how factors, such as contact duration, pH level, initial concentration of silver ions, and temperature affect the adsorption of silver ions. The equilibrium adsorption capacity (Q_e, measured in mg g^{-1}) was calculated using the equation below:

$$Q_e = (C_0 - C_e) \times V/m \quad (1)$$

where C_0 and C_e represent the initial and equilibrium concentrations of Ag+ (mg L^{-1}), respectively. V stands for the solution volume (L), and m corresponds to the mass of the sorbent (g). It is essential to note that each experiment was conducted in triplicate to ensure accuracy and reliability.

Subsequently, working solutions with the desired concentrations were prepared by diluting the stock solution with deionized water, ensuring precise control over the solution compositions for the experiments. The adsorption behaviour of silver ions (Ag+) was then investigated under various experimental conditions. To assess the impact of contact time, experiments were conducted at pH 6.9 with a silver ion concentration of 50 mg L^{-1}. The effect of solution acidity on silver ion removal efficiency was examined across a pH range of 2.0 to 10.0, using a silver ion concentration of 20 mgL^{-1}. To evaluate the influence of the initial silver ion concentration on adsorption capacity, different concentrations ranging from 10 to 200 mg L^{-1} were tested at a pH of 2.5. Additionally, the effect of temperature was studied at 20, 30 and 60 °C, while maintaining a dye concentration of 200 mg L^{-1}. Before mixing the suspensions, the pH of the initial solutions was carefully adjusted to the desired level using 0.1 M nitric acid and 0.1 M sodium hydroxide solutions.

RESULTS AND DISCUSSION

Sample characterization

Texture parameters

The N_2 adsorption/desorption isotherms observed for biomaterials RHC, C, EHC and EH closely resembled the type-IV classification outlined by IUPAC, indicative of a dominance of mesoporous characteristics (see Fig. 1). All isotherms displayed a gradual increase in the adsorbed amount of N_2 with rising relative pressure. The observed hysteresis loop for all four materials exhibited characteristics consistent with H3 type, typically associated with aggregates of plate-like particles or pores with slit-like structures.[24] The pore size distribution curves for all materials show the existence of mesopores with a relatively wide pore size distribution, especially for sample EH.

The textural parameters of all examined materials are summarized in Table 1. It is obvious that the treatment of EH results in an increase of BET surface area and pore volume of cellulose prepared from einkorn husks, Figure 1 (b). The sample EHC displays slightly higher values for the specific surface area and total pore volume. The calculated average pore diameters are in the range of 4-20 nm corresponding to a mesoporous structure. Considering the ionic diameter of Ag+ ions, which is 0.126 nm, the pore characteristics of the investigated biomaterials appear to be well-suited for overcoming diffusional limitations. This is because the pore channels allow silver ions to move through and interact with the sorbents efficiently during the adsorption process.

Determination of structure and surface morphology

The structural characteristics of the samples were determined by XRD. The pattern of cellulose, the well-known diffraction peaks at 2Θ 15.1°, 22.4° and 34.3° were attributed to the planes of (101), (002) and (040), respectively, all

of which were in agreement with the previously published data (Fig. 2).[25,26] The broadening of the curve at about 2Θ 28° observed for sample EH can be explained by the presence of amorphous lignin in its composition.

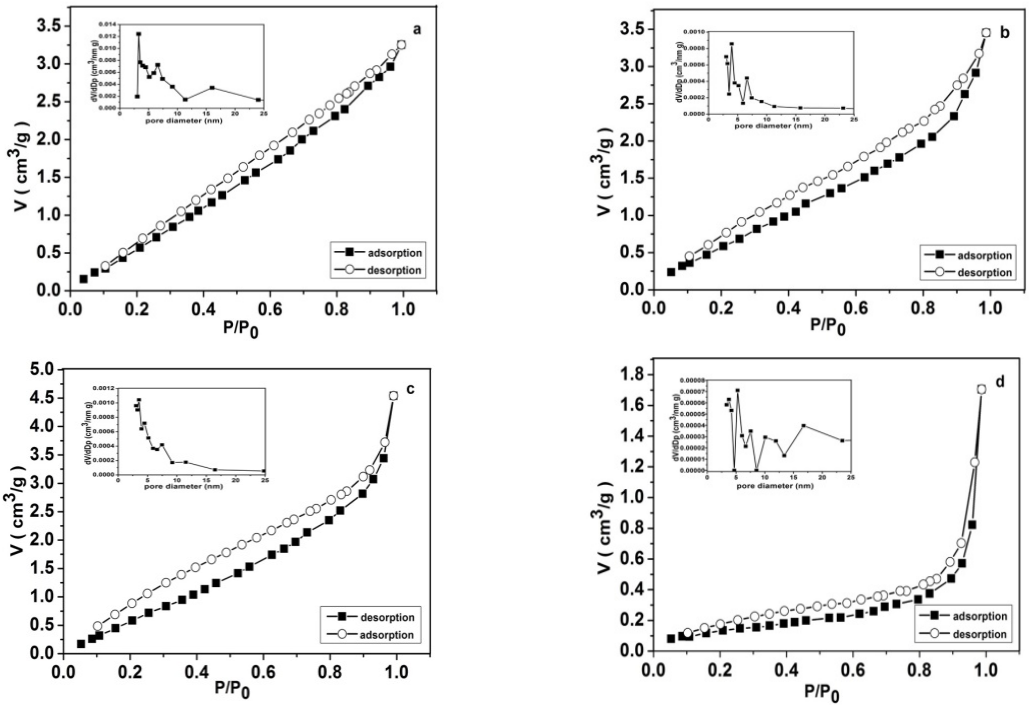

Figure 1: Nitrogen adsorption-desorption isotherms and pore size distribution of RHC (a); C (b); EHC (c); EH (d)

Table 1
Texture characteristics of the samples

Sample	S (m^2/g)	V (cm^3/g)	D_{av} (nm)	V_{mi} (cm^3/g)
RHC	4.5	0.005	4.4	0.001
C	3.0	0.005	6.7	0.001
EHC	5.5	0.007	6.8	0.001
EH	0.50	0.003	20.0	-

*S – BET-specific surface area; V – total pore volume; D_{av} – average pore diameter and V_{mi} – micropore volume

The type of characteristic surface functional groups in the samples was determined by FTIR analysis. The results are presented in Figure 3. The FTIR spectra of the three types of cellulose are similar. They contain the absorption bands characteristic of cellulose at 1057 cm^{-1} and 1383-1430 cm^{-1}, associated with the valence vibrations of the glucosidic chains' OH- and C-O groups that make up the polysaccharide. The presence of hemicelluloses, composed mainly of pentoses, and of lignin in the composition of raw einkorn husks makes the spectrum different from those of cellulosic materials. Pentoses contain compounds with a typical C=O group, with a characteristic absorption at 1650 cm^{-1} and a C-H bond (2857 and 2920 cm^{-1}). Lignin is a phenolic phenylpropanoid amorphous polymer composed of various aromatic rings and carbonyl groups, which determines the complex nature of its spectrum. Typical valence vibrations for lignin are those at 1464, 1726 and 1830 cm^{-1}.[27] It should be noted that the C-O and OH- groups are hydrophilic by nature. They will ensure a good wettability of the material with the aqueous solution of the modifying agent, in our case, $Ag(NO_3)$. The surface morphology of the biomaterials RHC, C, EHC and EH was investigated by SEM. The results are presented in Figure 4.

As can be seen, the texture of raw einkorn husks is dense and non-porous, whereas commercial cellulose and cellulose derived from rice and einkorn husks have a looser surface. This characteristic is essential for facilitating better contact between the sample and silver ions.

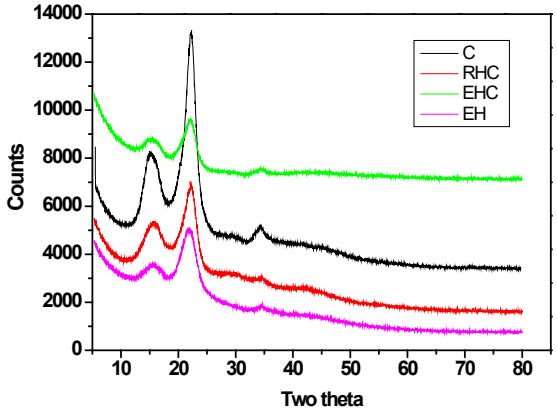

Figure 2: XRD diffractograms of the samples

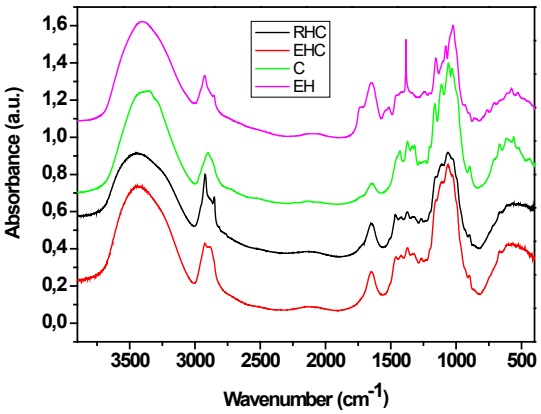

Figure 3: FTIR spectra of the samples

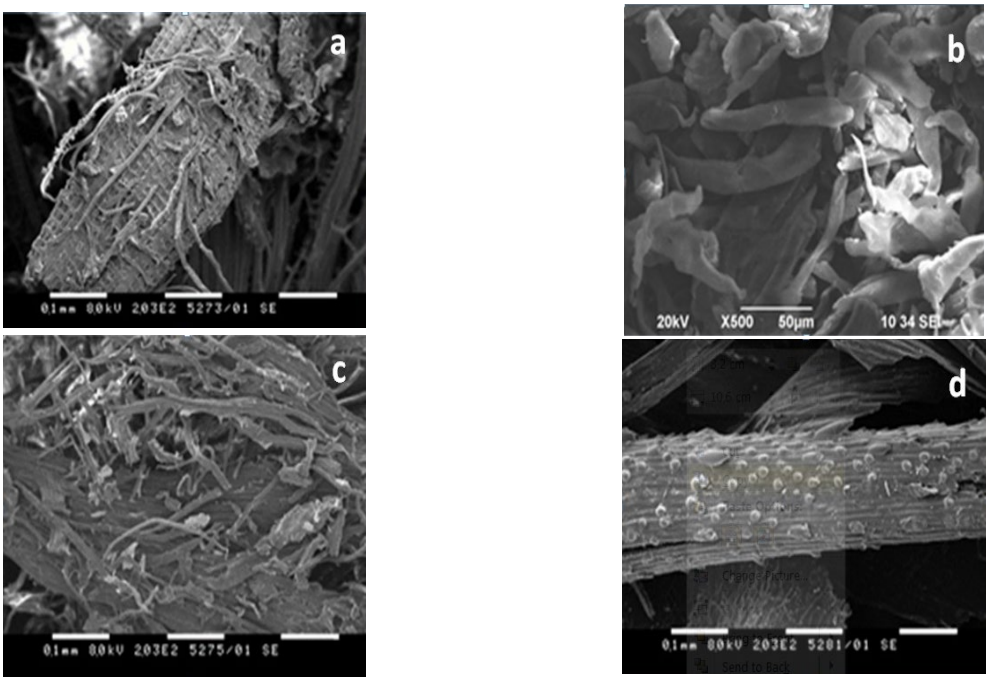

Figure 4: SEM micrographs of (a) RHC; (b) C; (c) EHC and (d) EH

Adsorption studies

Effect of contact time and adsorption kinetics

The relation between the amount of Ag^+ ions adsorbed and the time is presented in Figure 5. It is evident from the graphs that the sorption of silver ions increases rapidly with contact time, reaching a maximum value. However, further increases in contact time do not significantly alter the adsorption. Therefore, an optimum contact time of 15 minutes for all studied biomaterials was determined for the adsorption of Ag^+. The rapid attainment of equilibrium indicates a strong attraction between the investigated biosorbents and Ag^+ ions. This suggests that the biosorbents have high affinity for binding with Ag ions, leading to efficient removal from the solution.

The kinetics of metal ion adsorption was described using Lagergren's first-order and Ho and McKay pseudo-second-order rate equations.[28] The researchers employed the pseudo-first-order rate equation:

$$\log(Q_e - Q_t) = \log(Q_e) - (k_1/2.303)\, t \quad (2)$$

where k_1, Q_e, and Q_t represent the Lagergren rate constant of adsorption (min^{-1}), the amount of

metal ion adsorbed at equilibrium (mg g^{-1}), and the amount of metal ion adsorbed at any given time t (mg g^{-1}), respectively. The adsorption rate constant k_1 can be determined by analyzing the slope of the curves depicting $log\ (Q_e - Q_t)$ against time (t), with the results presented in Table 2.

Ho and McKay[28] utilized a pseudo-second-order rate equation to investigate adsorption kinetics:

$$t/Q_t) = (1/k_2 Q_e) + (1/Q_e)t \quad (3)$$

where k_2 represents the pseudo-second-order rate constant for adsorption (g mg^{-1} min^{-1}). This model is better suited to predict the kinetic behaviour of adsorption, with chemical sorption assumed to be the rate-controlling step. The rate constant k_2, Q_e, and correlation coefficient (r^2) are provided in Table 2.

A comparison between the pseudo-first and second-order kinetic models indicates that the adsorption of Ag^+ ions onto all studied biosorbents conforms well to pseudo-second-order kinetics, which is consistent with other findings reported in the literature.[17,1,19] This implies that the rate of the process relies on both the concentration of silver ions in the solution and the number of available adsorption sites on the surfaces of the biosorbents.[29]

To evaluate the importance of diffusion in governing the rate of silver ions adsorption on samples RHC, C, EHC, and EH, we utilized the diffusion kinetic equation proposed by Weber and Morris:[30]

$$Q_t = k_{id} t^{1/2} + C \quad (4)$$

where k_{id} (mg $g^{-1}min^{-1/2}$) represents the intraparticle diffusion constant and C is equilibrium capacity (mg g^{-1}).

The results from this kinetic analysis indicate that the adsorption process comprises several stages. The kinetics plot (figures not shown) displays two distinct linear regions, suggesting a complex adsorption mechanism. It is evident from the results that diffusion is not the limiting factor in determining the rate of silver adsorption in this case. These findings indicate that the process of adsorption depends on the quantities of both the substance dissolved (silver ions) and the material under study for its adsorption properties. Additionally, chemical reactions seem to play a significant role in controlling the speed of this process.[31]

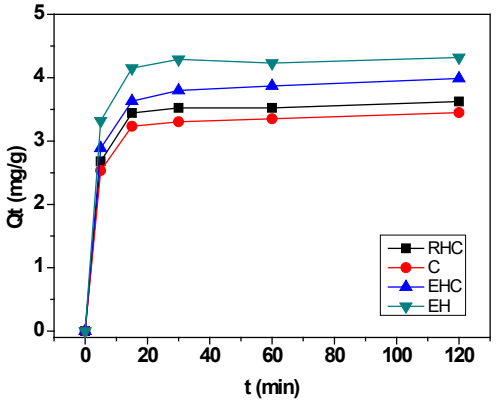

Figure 5: Effect of contact time on Ag^+ adsorption by samples RHC; C; EHC and EH

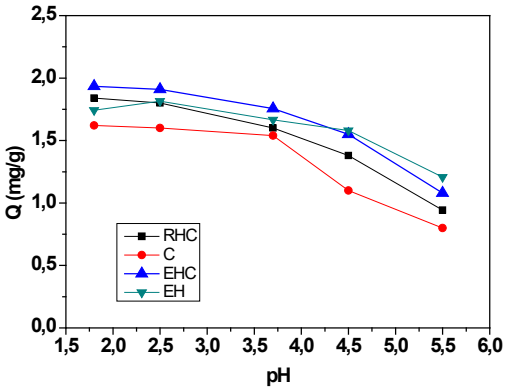

Figure 6: Effect of pH on Ag^+ adsorption by cellulose biosorbents

Table 2
Kinetic parameters for Ag^+ adsorption

Sample	Pseudo-first order constants			Pseudo-second order constants			Intra-particle diffusion constants		
	Q_e (mg g^{-1})	k_1 (min^{-1})	r^2	Q_e (mg g^{-1})	k_2 (g $mg^{-1}min^{-1}$)	r^2	k_{id} (mg g^{-1} $min^{-1/2}$)	C (mg g^{-1})	r^2
RHC	0.71	0.007	0.8904	3.80	0.550	0.9999	0.034	3.32	0.9773
C	1.49	0.014	0.9185	3.63	0.395	0.9996	0.015	3.39	0.7398
EHC	0.94	0.007	0.8178	4.06	0.450	0.9999	0.059	3.38	0.7776
EH	0.67	0.011	0.7985	4.36	0.949	0.9999	0.022	4.09	0.8285

Effect of pH

The pH value of the solution where adsorption takes place significantly influences the adsorption of silver ions onto various sorbents. Most research suggests that higher pH levels lead to greater adsorption of metal ions. However, our findings in this study contrast with this trend. Figure 6 illustrates that, as pH values increase, the amount of Ag^+ ions adsorbed decreases. This observation aligns with similar findings from other studies on silver ion adsorption onto rice husks.[1,19,32] The highest amounts of Ag^+ ions adsorbed on all the studied sorbents are observed in acidic media around pH 2-3. Consequently, a pH value of 2.5 was chosen as the optimal condition for Ag^+ adsorption.

Effect of temperature and thermodynamic studies

Exploring the impact of temperature on the adsorption of Ag^+ ions onto the four studied biosorbents from aqueous solutions is essential. The temperature alterations influence the sorption processes in two significant ways. Firstly, they lead to a decrease in the viscosity of the solution. Secondly, higher temperatures promote faster movement of metal ions in the solution, making them more readily available for sorption onto the sorbent material's surface and pores.[33]

Understanding the thermodynamic parameters of adsorption from solutions is important for gaining insights into the nature and mechanism of the adsorption process. These parameters shed light on the driving forces governing the interaction between the adsorbate and the adsorbent. By examining these thermodynamic parameters, researchers can assess the feasibility, spontaneity, and characteristics of the adsorption process, which is crucial for optimizing and comprehending its practical applications across various fields. To explore the impact of temperature on the removal of silver ions, experiments were conducted at 293 K, 303 K, and 333 K. The changes in Gibbs free energy (ΔG^0), enthalpy (ΔH^0), and entropy (ΔS^0) were determined using the following equations:

$$K_d = Q_e/C_e \quad (5)$$

$$\Delta G_0 = -RT\ln K_d \quad (6)$$

$$\ln K_d = \Delta S^0/R - \Delta H^0/RT \quad (7)$$

In the given formulas, K_d is the equilibrium constant, R represents the gas constant (measured in J $mol^{-1}K^{-1}$), and T denotes the temperature (measured in Kelvin). Plotting lnK_d against $1/T$ allows us to derive the enthalpy change, ΔH^0, from the graph's slope, and the entropy change, ΔS^0, from its intercept (as illustrated in Fig. 7).

The thermodynamic parameters ΔG^0, ΔH^0, and ΔS^0 are calculated and displayed in Table 3.

It was observed that, as the temperature increased, the amount of Ag^+ adsorbed on each biosorbent also increased. This phenomenon may be attributed to the acceleration of previously sluggish adsorption processes or the formation of new active sites on the surface of the sorbents.[19] This result also shows that the adsorption process is characterized as endothermic.

The variations in standard free energy at different temperatures exhibit negative values, indicating the feasibility and spontaneity of silver ion adsorption on biomaterials RHC, C, EHC, and EH. Comparatively, the ΔG^0 value for the Ag-EH system displays a more negative trend than the other three systems, implying more spontaneous adsorption of Ag^+ onto EH. Typically, ΔG^0 values for physisorption fall within the range of 0 to 20 kJ mol^{-1}, while chemisorption values range from 80 to 400 kJ mol^{-1}. The computed ΔG^0 values in this study affirm that physisorption predominates as the mechanism. Conversely, positive ΔH^0 values (ranging from 19.35 to 63.36 kJ mol^{-1}) confirm that adsorption is primarily physical, and the efficiency increases with rising temperature. As the entropy change (ΔS^0) is positive, it means that, as temperature rises, there is more disorder happening at the interface between the adsorbent and the solution. This also suggests that the attraction between the adsorbent and the adsorbate gets stronger.[34] This positive ΔS^0 value also suggests the irreversibility and stability of adsorption.[35,36] The slight positive ΔS^0 values observed in the studied systems imply minimal structural alterations on the adsorbent surfaces during the adsorption process.

Adsorption isotherm

Adsorption isotherms are crucial in understanding the behaviour of adsorbates on solid surfaces. They depict how the amount of adsorbate ions adsorbed onto the surface of the adsorbent varies with changes in concentration at a constant temperature. By studying these isotherms, adsorption mechanisms can be elucidated, porous materials can be characterized, and efficient adsorption processes can be designed for various applications. The experimental Ag^+ adsorption isotherms for the investigated materials are represented in Figure 8.

In this study, the equilibrium data concerning silver ions were scrutinized employing three prominent isotherm models: Langmuir, Freundlich, and Dubinin-Radushkevich models. The Langmuir model describes adsorption as a monolayer process, where adsorbate molecules form a single layer on the adsorbent surface with no interaction between adsorbed molecules. The Freundlich model, on the other hand, is an empirical equation that describes multilayer adsorption onto heterogeneous surfaces, allowing for variation in adsorption energies.

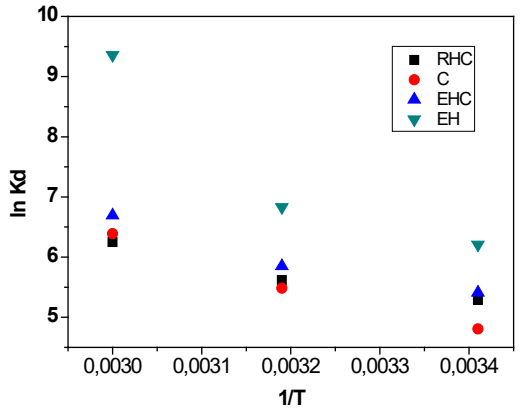

Figure 7: Plots of 1/T *vs.* $\ln K_d$ for adsorption of silver ions

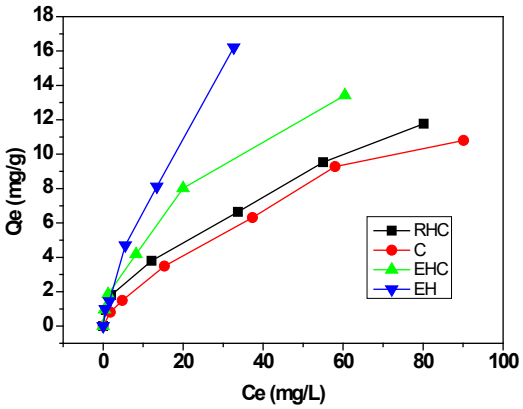

Figure 8: Experimental adsorption isotherms toward Ag^+ ions

Table 3
Change of the thermodynamic parameters with temperature

Adsorbent	ΔH^0 (kJ mol^{-1})	ΔS^0 (J mol^{-1} K^{-1})	ΔG^0 (kJ mol^{-1})		
			293 K	313 K	333K
RCH	19.35	109.33	-12.90	-14.00	-17.30
C	31.94	148.49	-12.01	-13.51	-18.01
EHC	25.77	132.24	-12.91	-14.23	-18.19
EH	63.36	266.21	-15.75	-18.45	-26.55

The Dubinin-Radushkevich model is used for physical adsorption onto heterogeneous surfaces, considering the adsorbent's micropore structure and the energy distribution of adsorption sites. These models provide insights into adsorption mechanisms and aid in optimizing adsorption processes in various industries. The linear forms of the above isotherm models are expressed by the equations:

Langmuir model: $C_e/Q_e = 1/K_L Q_0 + C_e/Q_0$ (8)

Freundlich model: $lnQ_e = lnk_F + (1/n)lnC_e$ (9)

Dubinin-Radushkevich model: $lnQ_e = lnQ_m - \beta\varepsilon^2$ (10)

where C_e is the equilibrium concentration of silver ions, Q_e is the amount of silver ions adsorbed per unit mass of adsorbent at equilibrium, Q_0 and Q_m are the maximum adsorption capacity, K_L is the Langmuir equilibrium constant, k_F is the Freundlich equilibrium constant, n is the Freundlich exponent, β is the adsorption energy constant, ε is the Polanyi potential.

The obtained isotherm constants and correlation coefficients, as presented in Table 4, reveal that the adsorption of silver ions onto the four cellulose biomaterials was effectively described by the Freundlich isotherm model. This is evidenced by the notably high correlation coefficients (r^2 exceeding 0.988), surpassing those obtained from the Langmuir and Dubinin–Radushkevich (D-R) isotherm models. A good fit of experimental data to the Freundlich model suggests that the adsorption process follows multilayer metal ions adsorption on heterogeneous surfaces, with relatively uniform energy distribution. However, it is important to recognize the empirical nature of the model, which may not capture all the complexities of the adsorption process in heterogeneous systems.

Cellulose biomaterials RHC, C and EHC exhibit similar adsorption capacities towards silver ions, while raw einkorn husks show the highest capacity for silver ions. This suggests that textural characteristics might not be the primary

factor influencing silver ion adsorption. Instead, it implies that the presence of various functional groups in the lignocellulosic EN sample could serve as additional active centres for adsorption, thus playing a crucial role in enhancing the adsorption of Ag^+ ions.

The values of "*n*" derived from the Freundlich isotherm model for the investigated biomaterials fall within the range of 1.43 to 1.95. This range suggests that the adsorption process is favourable for all four materials. According to Zhang *et al*.,[36] a higher value of *1/n* in the Freundlich model signifies a more uniform distribution of adsorption site energies on the adsorbent surface. When the *1/n* value approaches 1, adsorption tends to be more linear and less dependent on concentration. In this study, the data revealed that the nonlinearity of the isotherms, indicated by *1/n* values ranging from 0.51 to 0.70, varied among the four samples. Additionally, the analysis suggests that the surface of EH demonstrates a more uniform distribution of adsorption site energies compared to the other three samples.

In contrast, the Dubinin-Radushkevich isotherm model offers an understanding of adsorption energy. The computed mean free energy values range from 0.5 to 1.62 kJ mol^{-1}. These findings imply that the predominant adsorption mechanism is physisorption.

Table 4
Isotherm constants and correlation coefficients for silver adsorption

Sample	Langmuir parameters			Freundlich parameters			Dubinin-Radushkevich parameters		
	Q_0 (mg g^{-1})	K_1 (L mg^{-1})	r^2	k_F ($mg^{1-n}L^n$ g^{-1})	n (L mg^{-1})	r^2	$Q_{m(o)}$ (mg g^{-1})	E (kJ mol^{-1})	r^2
RHC	14.16	0.041	0.8803	1.72	1.84	0.9930	7.61	1.11	0.6757
C	15.63	0.023	0.9263	1.96	1.49	0.9969	5.83	0.51	0.6903
EHC	15.72	0.074	0.8970	1.60	1.95	0.9936	6.20	1.62	0.8211
EH	26.08	0.043	0.7836	1.34	1.43	0.9881	9.49	0.62	0.7399

Table 5
Atomic surface concentration of elements detected in the samples

Sample	C, at%	O, at%	Ag, at%	Si, at%
RHC	69.38	29.69	0.08	0.86
C	67.14	31.75	0.08	0
EHC	67.89	31.11	0.02	0.29
EH	79.04	15.18	0.02	2.92

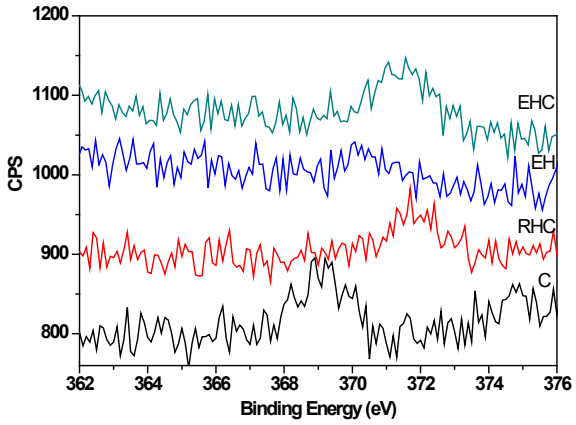

Figure 9: Photoelectron core level of studied materials after adsorption of Ag ions for Ag3d

XPS analysis of biosorbents after Ag(I) adsorption

X-ray photoelectron spectroscopy (XPS) was employed to analyze the surface composition and chemical states after adsorption. The results obtained are presented in Table 5 and Figure 9. Table 5 provides the atomic concentrations of the constituent elements observed on the surface of

all biomaterials following the adsorption of Ag^+ ions. The presence of silicon is due to the natural amorphous biogenic SiO_2 in the raw husks.

The confirmation of the adsorption process is supported by the presence of the Ag 3d peak in the scan. Figure 9 displays the Ag 3d photoelectron spectra for all the investigated biosorbents, providing insight into distinguishing silver in different oxidation states. However, determining the oxidation state of silver solely through its XPS peaks is challenging due to minimal chemical shifts. Generally, the binding energies of Ag $3d_{5/2}$ and Ag $3d_{3/2}$ are key indicators of silver presence.[37,38]

For sample C and sample EHC, the binding energies are measured at 368.2 eV and 368.3 eV, respectively. Notably, the doublet is shifted to a higher binding energy compared to metallic silver, as observed in sample RHC (369.0 eV and 375 eV). This shift may be ascribed to the phenomenon of "charge transfer states", as discussed in several studies.[39,40]

Additionally, positive core level shifts for Ag $3d_{5/2}$ have been documented for exceedingly small Ag particles, nearing 2 nm in diameter.[41] The separation between the two peaks of the silver 3d doublet was approximately 6 electron volts (eV), suggesting the formation of metallic silver.[42] Conversely, the Ag 3d doublet for sample EH exhibits a shift in the opposite direction, measuring at a negative 0.3 eV (367.9 eV and 371.6 eV), indicative of Ag_2O presence. These XPS findings underscore the intricate nature of Ag+ ion adsorption on the employed adsorbents, affirming the formation of metallic Ag-clusters on the surfaces of all examined materials.

We hypothesize that the adsorption of Ag^+ ions progresses through several stages, culminating in the formation of Ag^0. Thus, the adsorption process of Ag^+ ions can be described as follows:

$$Ag^+(\text{solution}) \text{ --- } Ag^+(\text{adsorbate}) \text{ --- } Ag_y^{n+}(\text{adsorbate}) \text{ --- } Ag^0(\text{adsorbate}) \quad (11)$$

The observed relationship between the amount of adsorbed silver and pH indicates that as pH increases, the quantity of adsorbed Ag^+ ions decreases. This is likely due to ion exchange between Ag^+ ions and the H^+ ions of the OH groups of the biosorbents, which facilitates the formation of Ag_y^{n+} clusters in subsequent stages. This confirms the adsorption mechanism observed with lignocellulosic materials derived from *Populus alba L.* and *Robinia pseudoacacia L.* [23]

The findings provide a basis for further research on cellulose materials investigated in this study, which will involve analyzing their antibacterial properties and activity when incorporating silver.

CONCLUSION

Silver has been effectively adsorbed onto cost-effective cellulose-based natural adsorbents derived from cereal by-products. The process follows pseudo-second-order kinetics. Low pH values favor silver adsorption. The calculated Gibbs free energy values confirm that physisorption is the predominant sorption mechanism. The isotherm constants and correlation coefficients reveal that silver ion adsorption onto the four cellulose biomaterials is effectively described by the Freundlich isotherm. A good fit of experimental data to this model suggests that the process involves multilayer metal ions adsorption on heterogeneous surfaces with relatively uniform energy distribution. Cellulose biomaterials RHC, C, and EHC demonstrate comparable abilities to adsorb silver ions, whereas untreated einkorn husks exhibit the highest capacity for silver ions. The XPS results highlight the complex process of Ag^+ ion adsorption on the tested adsorbents, confirming the creation of metallic Ag-clusters on their surfaces. The stable controlled deposition of silver on natural supports offers an opportunity to create materials with potential bactericidal properties.

ACKNOWLEDGEMENTS: Research equipment of the Distributed Research Infrastructure INFRAMAT, part of the Bulgarian National Roadmap for Research Infrastructures, supported by the Bulgarian Ministry of Education and Science, was used in this investigation.

REFERENCES

[1] X. Luo, X. Lin, X. Luo, A. Luo and X. Liang, *Mater. Sci. Forum.*, **658**, 45 (2010), https://doi.org/10.4028/www.scientific.net/MSF.658.45

[2] T. Jintakosola and W. Nitayaphat, *Mater. Res.*, **19**, 1114 (2016), http://dx.doi.org/10.1590/1980-5373-MR-2015-0738

[3] A. Muñoz, F. Espínola, E. Ruiz, M. Moya and E. Castro, *Nanomaterials-Basel*, **13**, 295 (2023), https://doi.org/10.3390/nano13020295

[4] M. Yoo-iam, R. Chaichana and T. Satapanajaru, *Chem. Speciat. Bioavailab.*, **26**, 257 (2014), https://doi.org/10.3184/095422914X1414433220557

[5] M. Akter, T. Sikder, M. Rahman, A. Ullah, K. Hossain *et al*., *J. Adv. Res*., **9**, 1 (2018), https://doi.org/10.1016/j.jare.2017.10.008
[6] H. Akmal and A. Umar, in "Nanobiotechnology for Plant Protection, Green Synthesis of Silver Nanomaterials", edited by A. Kamel, K. Abd-Elsalam, Elsevier, Amsterdam, The Netherlands, 2022, pp. 627–647
[7] E. Kirkova, "Chemistry of the Elements and Their Compounds", University Publishing House St. Kliment Ohridski (in Bulgarian), 2007, ch. 11
[8] A. Landsdown, *Curr. Probl. Dermatol*., **33**, 17 (2006), https://doi.org/10.1159/000093928
[9] A. Rizki, J. Rahmi and H. Hira, *J. Nat*., **20**, 6 (2020), https://doi.org/10.24815/jn.v20i1.12016
[10] H. Almas, M. Nawshad, N. Ayesha, G. Moinuddin, I. Jibran *et al*., *CBEN*, **4**, 240 (2017), https://doi.org/10.1002/cben.201700002
[11] A. Mudasir, A. Shakeel, S. Babu and I. Saiqa, *Int. J. Pharm*., **2**, 280 (2015), https://doi.org/10.13040/IJPSR.0975-8232.IJP.2(6)
[12] G. Parikshit, B. Richard, T. Jim and W. Patrick, *Cellulose*, **18**, 1063 (2011), https://doi.org/10.1007/s10570-011-9540-0
[13] M. Sulyman, J. Namiesnik and A. Gierak, *Pol. J. Environ. Stud*., **26**, 479 (2017), https://doi.org/10.15244/pjoes/66769
[14] S. Uzunova, L. Minchev, I. Uzunov and V. Toteva, *Chem. Eco*., **32**, 976 (2016), https://doi.org/10.1080/02757540.2016.1212850
[15] K. Asemave, L. Thaddeus and P. Tarhemba, *Sustain. Chem*., **2**, 271 (2021), https://doi.org/10.3390/suschem2020016
[16] P. Vassileva, I. Uzunov and D. Voykova, *Cellulose Chem. Technol*., **56**, 1117 (2022), https://doi.org/10.35812/CelluloseChemTechnol.2022.56.100
[17] S. Zafar, N. Khalid and M. Mirza, *Separ. Sci. Tehnol*., **47**, 1793 (2012), https://doi.org/10.1080/01496395.2012.657322
[18] S. Zafar, N. Khalid and M. Mirza, *The Nucleus*, **48**, 323 (2011)
[19] S. Zafar, M. Khan, A. Shanableh, S. Ahmad, S. Manzoor *et al*., *Desalin. Water Treat*., **236**, 108 (2021), https://doi.org/10.5004/dwt.2021.27683
[20] F. Unglaube, A. Lammers, C. Kreyenschulte, M. Lalk and E. Mejía, ChemistryOpen, **10**, 1244 (2021), https://doi.org/10.1002/open.202100239
[21] T. Radoykova, T. Angelova, P. Vassileva, N. Georgieva, A. Detcheva *et al*., *Cellulose Chem. Technol*., **53**, 427 (2019), https://doi.org/10.35812/CelluloseChemTechnol.2019.53.43
[22] P. Vassileva, T. Radoykova, A. Detcheva, I. Avramova, K. Aleksieva *et al*., *Int. J. Environ. Sci. Technol*., **3**, 1319 (2016), https://doi.org/10.1007/s13762-016-0970-y
[23] P. Vassileva, A. Detcheva, T. Radoykova, I. Avramova, K. Aleksieva *et al*., *Cellulose Chem. Technol*., **52**, 633 (2018), https://www.cellulosechemtechnol.ro/pdf/CCT7-8(2018)/p.633-643.pdf
[24] E. Moawed, M. Eissa and S. Al-Tantawy, *Int. J. Environ. Sci. Technol*., **20**, 7767 (2023), https://doi.org/10.1007/s13762-022-04428-w
[25] J. Gong, J. Li, J. Xu, Z. Xiang and L. Mo, *RSC Adv*., **7**, 33486 (2017), https://doi.org/10.1039/C7RA06222B
[26] H. Spurlin and M. Grafflin, in "Cellulose and Cellulose Derivatives", edited by E. Ott, N. Bikales and L. Segal, Interscience Publishers, New York, 1971
[27] R. Bezerra, M. Silva, A. Morais, J. Osajima, M. Santos *et al*., *Materials*, **7**, 7907 (2014), https://doi.org/10.3390/ma7127907
[28] R. Emmanuel, D. Fortela, W. Sharp, R. Hernandez and M. Zappi, *Clean Eng. Technol*., **1**, 100032 (2020), https://doi.org/10.1016/j.clet.2020.100032
[29] P. Vassileva, D. Voykova, I. Uzunov and S. Uzunova, *Comptes Rendus Acad. Bulg. Sci*., **71**, 1192 (2018), https://doi.org/10.7546/CRABS.2018.09.05
[30] W. Weber and J. Morris, *J. Sanit. Eng. Div. Am. Soc. Civ. Eng*., **89**, 31 (1963), https://doi.org/10.1061/JSEDAI.0000430
[31] A. Dwivedi, S. Dubey, M. Sillanpää, H. Liimatainen, T. Suopajärvi *et al*., *Int. J. Biol. Macromol*., **76**, 109 (2015), https://doi.org/10.1016/j.ijbiomac.2015.02.032
[32] S. Yefremova, A. Kablanbekov, B. Satbaev and A. Zharmenov, *Materials*, **16**, 7353 (2023), https://doi.org/10.3390/ma16237353
[33] P. Staroń, J. Chwastowski and M. Banach, *J. Clean Prod*., **149**, 290 (2017), https://doi.org/10.1016/j.jclepro.2017.02.116
[34] F. Arias, M. Guevara, T. Tene, P. Angamarca, R. Molina *et al*., *Nanomaterials*, **10**, 681 (2020), https://doi.org/10.3390/nano10040681
[35] M. Sahmoune, *Environ. Chem. Lett*., **17**, 697 (2019), https://doi.org/10.1007/s10311-018-00819-z
[36] D. Zhang, Q. Luo, B. Gao, S. Chiang, D. Woodward *et al*., *Chemosphere*, **144**, 2336 (2016), https://doi.org/10.1016/j.chemosphere.2015.10.124
[37] S. Chook, C. Chia, S. Zakaria, M. Ayob, K. Chee *et al*., *Nanoscale Res. Lett*., **7**, 541 (2012), https://doi.org/10.1186/1556-276X-7-54
[38] K. Hsu and D. Chen, *Nanoscale Res. Lett*., **9**, 193 (2014), https://doi.org/10.1186/1556-276X-9-193
[39] H. Li, M. Wang, Y. Li, F. Mo, L. Zhu *et al*., *Appl. Surf. Sci*., **562**, 150168 (2021), https://doi.org/10.1016/j.apsusc.2021.150168
[40] X. Huang, P. Jain, I. El-Sayed and M. El-Sayed, *Nanomedicine*, **2**, 681 (2007), https://doi.org/10.2217/17435889.2.5.681
[41] S. Link and M. El-Sayed, *J. Phys. Chem. B*, **103**, 8410 (1999), https://doi.org/10.1021/jp9917648
[42] J. Ma, J. Zhang, Z. Xiong, Y. Yong and X. Zhao, *J. Mat. Chem*., **21**, 3350 (2011), https://doi.org/10.1039/C0JM02806A